THE JOURNAL OF PHYSICAL CHEMISTRY A
A JOURNAL OF THE AMERICAN CHEMICAL SOCIETY

pubs.acs.org/JPCA

Article

Ultrasmall Cluster Model for Investigating Single Atom Catalysis: Dehydrogenation of 1-Propanamine by Size-Selected $Pt_1Zr_2O_7$ Clusters Supported on HOPG

Published as part of The Journal of Physical Chemistry virtual special issue "Honoring Michael R. Berman".

Michael A. Denchy, Linjie Wang, Benjamin R. Bilik, Lucas Hansen, Sandra Albornoz, Francisco Lizano, Nicolas Blando, Zachary Hicks, Gerd Gantefoer, and Kit H. Bowen*

Cite This: *J. Phys. Chem. A* 2022, 126, 7578−7590

Read Online

ACCESS | Metrics & More | Article Recommendations | Supporting Information

ABSTRACT: The selective dehydrogenation of hydrocarbons and their functionalized derivatives is a promising pathway in the realization of endothermic fuel systems for powering important technologies such as hypersonic aircraft. The recent surge in interest in single atom catalysts (SACs) over the past decade offers the opportunity to achieve the ultimate levels of selectivity through the subnanoscale design tailoring of novel catalysts. Experimental techniques capable of investigating the fundamental nature of the active sites of novel SACs in well-controlled model studies offer the chance to reveal promising insights. We report here an approach to accomplish this through the soft landing of mass-selected, ultrasmall metal oxide cluster ions, in which a single noble metal atom bound to a metal oxide moiety serves as a model SAC active site. This method allows the preparation of model catalysts in which monodispersed neutral SAC model active sites are decorated across an inert electrically conductive support at submonolayer surface coverage, in this case, $Pt_1Zr_2O_7$ clusters supported on highly oriented pyrolytic graphite (HOPG). The results contained herein show the characterization of the $Pt_1Zr_2O_7$/HOPG model catalyst by X-ray photoelectron spectroscopy (XPS), along with an investigation of its reactivity toward the functionalized hydrocarbon molecule, 1-propanamine. Through temperature-programmed desorption/reaction (TPD/R) experiments it was shown that $Pt_1Zr_2O_7$/HOPG decomposes 1-propanamine exclusively into propionitrile and H_2, which desorb at 425 and 550 K, respectively. Conversely, clusters without the single platinum atom, that is, Zr_2O_7/HOPG, exhibited no reactivity toward 1-propanamine. Hence, the single platinum atom in $Pt_1Zr_2O_7$/HOPG was found to play a critical role in the observed reactivity.

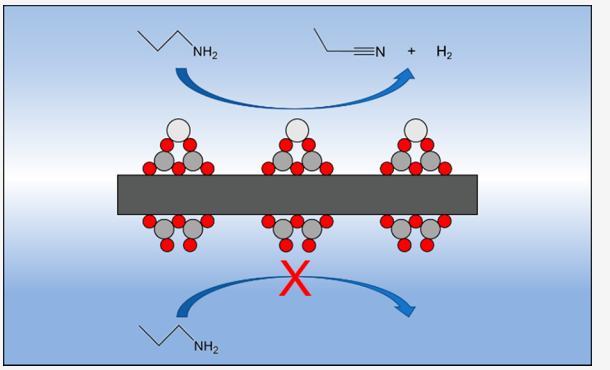

INTRODUCTION

Endothermic fuel systems are increasingly attractive for their potential role in a variety of technological applications, such as in hypersonic aircraft.[1,2] Such systems require molecular species that can absorb energy to undergo a transformation into product species which are either themselves consumable as fuel or, at the very least, not inhibitive to successive conversion cycles. Much of the work in this area has focused on the thermal decomposition of hydrocarbons.[3,4] Of particular promise is the selective dehydrogenation of hydrocarbons, i.e., the dehydrogenation of alkanes to alkenes, which in principle can make effective use of excess thermal energy present in the system to drive the formation of partially dehydrogenated hydrocarbons and H_2.[5−7] The selective dehydrogenation of alkanes to alkenes requires the activation and cleavage of C−H bonds, which typically have a greater bond enthalpy than the C−C bonds within a given alkane molecule. This presents a serious problem during the elevated temperatures required in applications like that of endothermic fuel systems, in which the thermal cracking resulting from C−C bond cleavage is especially problematic. Hence, the use of a proper catalyst, promoting the selective activation and cleavage of C−H bonds, while minimizing the propensity for breaking C−C bonds, is therefore required in such applications.

C−H bonds are known to be closed-shell σ orbitals,[8] requiring activation via a metal or metal oxide catalyst to accomplish practical selective dehydrogenation.[9] By far the most prominent metal catalyst species used for the selective

Received: May 6, 2022
Revised: August 22, 2022
Published: October 18, 2022

dehydrogenation of hydrocarbons has been platinum.[10] Commercial platinum-based catalysts employed for alkane dehydrogenation have generally consisted of platinum particles supported on a metal oxide, typically Al_2O_3.[11] In these catalysts, the active platinum species are in the form of small nanoparticles dispersed across the metal oxide support.[12] Such small particles offer a variety of platinum atoms in different coordination environments as opposed to the extended planar facets of large particles and single crystal surfaces. For many heterogeneous catalytic systems, it has long been hypothesized,[13,14] and in some cases already well-evidenced,[15] that coordinatively unsaturated metal atoms associated with defect sites are the primary drivers of catalytic activity. In small Pt nanoparticles, there is a significant relative amount of both coordinatively saturated and unsaturated atoms, associated with terrace sites and step/edge sites, respectively—all of which can contribute to observed activity and selectivity. Further complicating the picture, it has even been shown that for hydrocarbons of different sizes, different activity and selectivity effects can be demonstrated for given active sites.[16] In all known cases, some specific active site is able to activate a host of undesirable side reactions, including thermal cracking, overdehydrogenation, isomerization, and polymerization.[17] One long-standing goal of research in this area has been to understand and minimize these effects.

Even in the presence of a catalyst, dehydrogenation of hydrocarbons requires significant energy input, introducing the potential for coking, i.e., the formation of soot-like carbonaceous deposits, which is known to deactivate catalyst surfaces[18,19] and cause overheating problems in fuel systems.[20] In addition to thermal cracking of hydrocarbons into decreasingly smaller fragments, overdehydrogenation, leading to the formation of alkyne species, is also problematic. There is broad consensus that surface-bound alkyne species are likely coking precursors,[21] and as such, the avoidance of coking requires the selective dehydrogenation of hydrocarbons to alkenes, without further dehydrogenation to alkynes. There has been work devoted to elucidating the coking propensity for a wide variety of platinum-containing systems, ranging from well-controlled ultrahigh-vacuum (UHV) studies with model catalysts, including single crystal surfaces,[22,23] to studies of commercial supported nanoparticle catalysts.[24−26]

Especially innovative work by Baxter et al., sought to determine the onset of coking propensity for ultrasmall, size-selected platinum clusters supported on typical oxide surfaces.[27] A comparison of the ethylene dehydrogenation activity of samples prepared by depositing monodispersed Pt_4, Pt_7, or Pt_8 clusters on Al_2O_3 thin films showed that the Pt_7 clusters were especially prone to coking, whereas the Pt_4 and Pt_8 clusters were not. Supporting theoretical calculations suggested this observed effect was a result of the accessibility of a flat, single-layer cluster geometry for Pt_7 clusters supported on Al_2O_3, allowing a larger number of binding sites active for ethylene dehydrogenation.

Another theoretical investigation sought to compare the observed activities and selectivities for the dehydrogenation of *n*-alkanes, ranging in size from ethane to hexane, over two distinct forms of platinum, namely, a Pt(111) surface and a Pt_{55} cluster having a diameter of approximately 1 nm.[28] The results showed that undercoordinated Pt atoms typical of Pt clusters and small nanoparticles demonstrate higher activity for alkane dehydrogenation, but poorer selectivity to forming an alkene which can subsequently readily desorb. This is in agreement with experimental studies which have found the same effects for propane dehydrogenation, namely, an inverse relationship between activity and selectivity with platinum nanoparticle size in the 1−10 nm size regime.[12,16]

Especially useful insights into the role of both geometric and electronic structure of various platinum morphologies on alkane dehydrogenation have been gleaned by fundamental studies of the effects of promoter species included to augment the catalytic properties of platinum-based catalysts. Promoters have been shown to inhibit side reactions by limiting the domain size of the active metal surface[29−31] and by reducing the activity of step edges and corner sites.[32] This ability points toward any ensembles of particularly active atoms, even of the undercoordinated variety, being potentially problematic from the standpoint of selectivity. Another type of effect involves changes to the electronic structure of active sites by the presence of a promoter species, which can either involve changes to the electron density of the active site platinum atoms or a band gap alteration.[33]

These effects have been demonstrated down to the smallest size scales in additional work on size-selected supported platinum clusters involving nanoalloying of Pt_7 clusters with either boron[34] or tin[35−37] atoms in an attempt to suppress the coking propensity of the cluster. Incorporation of boron resulted in a cluster that less strongly binds ethylene and is less active for ethylene dehydrogenation, whereas tin resulted in almost complete suppression of ethylene dehydrogenation without reducing the actual binding energy of ethylene. Clearly, electronic and geometric effects can profoundly influence the observed dehydrogenation activity and selectivity of even the smallest assemblies of platinum atoms.

Though much useful knowledge has been gleaned about alkane dehydrogenation over the years, one promising avenue worth consideration for endothermic fuel applications is the use of functionalized hydrocarbons, chosen specifically to bolster the selective endothermic properties of the primary fuel. If properly transformed during the catalytic cycle, such species could potentially give an even higher yield of useful H_2, while forming a product species that is especially resistant to coking and other side reactions. Recent work by Gorte et al. demonstrated the endothermic dehydrogenation of 1-propanamine (1-PA) over a ZrO_2 powder catalyst to selectively produce propionitrile and H_2.[38] This reaction, performed at realistic elevated pressure and temperature conditions, was shown to be highly endothermic and catalytic, with promising activity and selectivity. H_2 formed via such a process could go on to be used as a fuel in a subsequent stage, whereas the nitrile formed constitutes a product species that should be relatively resistant to undesired side processes at elevated temperatures,[39] like coking. Hence, the dehydrogenation of functionalized hydrocarbon species like 1-PA over model catalysts merits further investigation at a more fundamental level.

New advances in the nanoscale design tailoring of heterogeneous catalysts offers a chance to further exploit the exotic effects of ultrasmall platinum species. Over the past decade, the long-speculated small-size limit of heterogeneous catalysis, namely, single atom catalysis (SAC), has been convincingly demonstrated.[40−42] The use of an isolated single metal atom, anchored to a support structure, as the catalytically active site offers the prospect of high selectivity for a wide range of chemical reactions.[43,44] Such systems have the added benefit of maximizing the surface-to-volume ratio of active

https://doi.org/10.1021/acs.jpca.2c03149
J. Phys. Chem. A 2022, 126, 7578−7590

species and thereby limiting the amount of expensive precious metal material required to produce a functional catalyst. Moreover, these systems constitute the epitome of interfacial effects, where the interaction between the single metal atom and nearby support atoms can have an especially pronounced effect on reactivity. Much attention has been paid to SACs of platinum on various supports in recent years, as it is both a widely used catalytic metal and quite expensive.[45] In the context of this study, the combination of single platinum atoms and ZrO_2 species is especially relevant because of the ability of Pt[46] and ZrO_2[47,48] each individually to catalyze dehydrogenation reactions, as well as because of the widely known excellent thermal stability of ZrO_2 as a support material.

Modeling SAC Active Sites with Small Supported Clusters. By their nature, real SAC systems exhibit a very low metal loading, typically <1 wt % of the single atom metal species. Hence, the vast majority of the atoms composing the metal oxide support have no interaction with the dispersed single metal atoms decorating the surface, making interrogation of the metal−support interface by spectroscopic means highly cumbersome and in many cases intractable. Our concept is to use ultrasmall clusters, wherein a single metal atom is bound to a metal oxide moiety acting as a small portion of the larger metal oxide support, to model isolated active sites of bulk SAC systems. This concept is illustrated below in Scheme 1.

Scheme 1. Illustration Showing an Example of a Bulk Metal-Oxide Supported Single Atom Catalyst and Its Corresponding Small Cluster Model

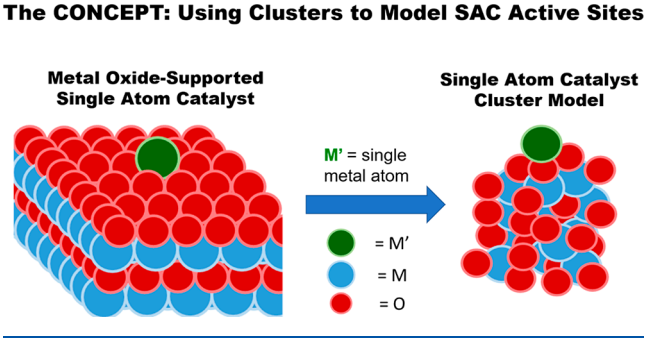

These clusters, prepared in the gas phase as ions, can then be interrogated by mass spectrometry, and subsequently mass-selected and soft-landed with low kinetic energy, onto a prepared, electrically conductive, cooled substrate, allowing for charge neutralization of the cluster ion to give the corresponding neutral species. A combination of soft landing and low substrate temperature helps to ensure the preservation of the clusters' structural integrity upon deposition. If the choice of substrate is made such that cluster−support interactions are minimized, the properties of a supported neutral cluster will be primarily governed by its own internal structure, allowing it to more properly mimic an SAC active site. Maintaining a low, submonolayer cluster coverage suppresses the possibility of agglomeration, at least during initial preparation and reactivity experiments, making it more likely that the clusters decorating the surface retain the stoichiometry selected for in the gas phase. A particular advantage of this fundamental approach is that all active atoms in prepared cluster model samples are confined to the topmost surface layer of the substrate, allowing for maximal signal during spectroscopic investigations. By comparison, many bulk SAC systems prepared through other synthetic methods have the active single atom dispersed throughout a porous material or around the three-dimensional structure of much larger nanoparticles. This can often make spectroscopic investigations rather cumbersome and can prevent crucial information about the SAC active site from being readily attainable.

There have been recent reports of SAC materials making use of small clusters as support moieties for an active single metal atom, albeit via an approach wholly different from the experimental concept we propose here. In these works, single metal atoms were preferentially decorated onto the metal oxide cluster nodes of various metal organic frameworks (MOFs).[49−55] Although these materials are structurally distinct from our model samples involving single metal-atom doped metal oxide clusters monodispersed on a crystal support surface, in that the cluster nodes are coordinated within an organic ligand framework, the spirit of the approach is similar. Many of these studies involved the isolation of a single metal atom, having positive charge character, onto a zirconium oxide hexamer cluster node, through which various reactions including ethylene hydrogenation,[49] nitrophenol reduction,[55] CO oxidation,[50] and others were demonstrated. Moreover, the demonstration of real materials in which fairly small metal oxide clusters decorated with a single metal atom serve as the active species further motivates fundamental single atom-doped cluster studies of the kind we report here.

Herein, we report our first application of this experimental approach to investigate the dehydrogenation of 1-PA on a prepared $Pt_1Zr_2O_7$ SAC model cluster system. To our knowledge, this is the first reported instance of the use of surface supported heteroatomic metal oxide clusters to model the active site of an SAC material. Cluster anions synthesized in a combined magnetron sputtering/inert gas condensation source were transported along an ion optical beamline, analyzed and mass-selected via quadrupole mass spectrometry, and soft-landed onto a prepared highly oriented pyrolytic graphite (HOPG) substrate maintained at 100 K under UHV conditions. The model catalysts were characterized by X-ray photoelectron spectroscopy (XPS), and their reactivity toward 1-PA was investigated via temperature-programmed desorption/reaction (TPD/R). XPS measurements acquired before and after TPD/R experiments served to provide additional insight into the reaction occurring on the model catalysts. The role of the single Pt atom was evidenced by comparing the reactivity observed for the $Pt_1Zr_2O_7$/HOPG system with that of Zr_2O_7/HOPG, lacking the single Pt atom. It was found that the presence of the single Pt atom is critical in defining the reactivity toward 1-PA, with $Pt_1Zr_2O_7$/HOPG exhibiting dehydrogenation of 1-PA to propionitrile and H_2, whereas the Zr_2O_7/HOPG system was inactive, deviating from the activity reported previously for bulk ZrO_2 powder catalysts.

EXPERIMENTAL METHODS

This work was conducted using a newly constructed apparatus with substantial improvements over its predecessor, the latter of which was used in previously published work from our laboratory[56−58] and described in detail previously.[59] The cluster ion beamline was completely redesigned, and the cluster deposition/surface analytical region of the apparatus underwent significant modification, while retaining much of the same analytical instrumentation. A detailed description of

https://doi.org/10.1021/acs.jpca.2c03149
J. Phys. Chem. A 2022, 126, 7578−7590

the newly constructed apparatus is given in the Supporting Information.

Sample Preparation. The beams of metal oxide cluster anions used in preparing samples were synthesized using our magnetron sputtering/inert gas condensation cluster source, the operative principles of which have been described previously.[S1] Both single atom Pt-doped zirconium oxide cluster anions, $Pt_1Zr_xO_y^-$, and the corresponding zirconium oxide cluster anions without the single Pt atom, $Zr_xO_y^-$, were synthesized via reactive magnetron sputtering using a gas mixture of argon (Airgas, 99.999%) and helium (Airgas, 99.999%), administered via dosing valves (Leybold 28341) each with a backing pressure of 30 psi, seeded with oxygen (Airgas, 99.994%) using a precision dosing valve (INFICON, VDH016-x) with an O_2 backing pressure of 15 psi. The $Pt_1Zr_2O_7^-$ species were formed using a pure zirconium metal sputtering target (Kurt J. Lesker, grade 702) onto which several thin Pt metal strips (1 × 10 mm) were spot-welded within the sputtered region of the target. The $Zr_xO_y^-$ species were formed using a pure zirconium metal sputtering target (Kurt J. Lesker, grade 702) with no Pt present.

After a cluster anion beam was generated, it was guided by the beamline optics to the inlet of the in-line QMF, where the beam composition was analyzed, and the chosen cluster stoichiometry was mass-selected with suboxygen resolution. Following mass selection, the cluster anions were guided and focused onto a grounded HOPG substrate (Bucker, ZYB grade, 12 × 12 mm^2, 2 mm thickness) with an estimated deposition spot size of ∼5 mm in diameter, under soft-landing conditions (<1 eV/atom). The substrate was prepared via mechanical exfoliation in air, and immediately transferred to UHV, where it was annealed (T = 773 K, Δt = 50 min) to ensure a clean surface. Surface cleanliness was confirmed via XPS, and an example survey spectrum of postannealed HOPG is shown in the Supporting Information (Figure S1). Because of the conductive nature of the substrate, cluster anions lost their charge to the surface upon deposition to become neutral clusters. A digital picoammeter (Keithley 6514) controlled by a custom Labview program designed in-house was used to monitor the resulting cluster discharge current and allowed a retarding bias voltage (−10 V) to be applied to the HOPG substrate surface via an external power supply to ensure soft-landing conditions for the cluster anions. Integration of the measured cluster discharge current over time allowed the calculation of the total number of clusters deposited for a given preparation, assuming one unit of elementary charge per cluster. Samples in the experiments reported here were typically prepared by depositing 5 × 10^{13} mass-selected clusters onto the HOPG substrate surface. The time required to accomplish a full deposition of this cluster coverage was typically ∼3 h with readily achievable mass-selected cluster anion intensities within our system.

Samples of 1-PA (Sigma-Aldrich, ≥99%) were prepared by loading a vessel with ∼1 mL of liquid and attaching it to a bakeable stainless steel vapor dosing setup. 1-PA samples were purified via several freeze−pump−thaw cycles using liquid nitrogen.

X-ray Photoelectron Spectroscopy. XPS measurements were acquired using the nonmonochromatic Mg Kα X-rays (1256.3 eV) generated via the Mg/Al dual anode X-ray source to induce core electron photoemission in the samples, and the kinetic energies of photoemitted electrons were analyzed via the hemispherical electron energy analyzer. All XPS spectra reported were calibrated to a graphitic carbon 1s binding energy value of 284.5 eV. Quantitative data analysis and peak model fitting was performed using CasaXPS (Casa Software Ltd.) software.

Carbon 1s (C 1s) spectra were numerically fitted using an asymmetric Gaussian-broadened Lorentzian peak (A-(0.4,0.38,20)GL(20)) for the C 1s transition arising from sp^2-hybridized graphitic carbon and a symmetric Gaussian-broadened Lorentzian (GL(30)) peak for the satellite peak corresponding to the $\pi-\pi^*$ transition in HOPG. A full width half-maximum (fwhm) of ∼1.6 eV was obtained for the sp^2 C 1s peaks in all spectra. Oxygen 1s (O 1s) spectra were numerically fitted using Gaussian-broadened Lorentzian peaks (GL(30)) following linear background subtraction. A fwhm of 2−2.3 eV was allowed during initial fitting, with an optimal value of 2.20 eV obtained and thereby constrained for all spectra. Zirconium 3d (Zr 3d) and platinum 4f (Pt 4f) spectra were each numerically fitted with sets of Gaussian-broadened Lorentzian peaks (GL(30)), following Shirley background subtraction. The Zr 3d peak pair was constrained to have an integrated peak area ratio of 3:2 corresponding to the $3d_{5/2}$ and $3d_{3/2}$ states, and a spin−orbit splitting of 2.43 eV. The Pt 4f peak pair sets were each constrained to have an integrated peak area ratio of 4:3, corresponding to the $4f_{7/2}$ and $4f_{5/2}$ states, and a spin−orbit splitting of 3.33 eV. A fwhm of 1.7−2.5 eV was allowed during initial fitting for both Zr 3d and Pt 4f spectra, with an optimal value of 2.2 eV obtained for each. The constraints for each species were maintained for the fitting of all XPS acquired using a constant analyzer pass energy of 71.55 eV.

Temperature-Programmed Desorption/Reaction. TPD/R experiments were performed by heating prepared samples at a well-controlled linear rate of 1 K/s, positioned in front of the inlet aperture of the low-profile ionization region of the QMS. Temperature programming was accomplished by resistive heating of the HOPG substrate via the current generated by an external power supply (Sorensen DCS 55-55) driven by a programmable PID controller (Eurotherm 2048) interfaced with a thermocouple temperature−voltage converter (Dataexel, DAT4531A) connected to the K-type thermocouple monitoring the substrate temperature. Dosing of 1-PA was accomplished using a variable leak valve (Varian, 951-5106) and simultaneously monitoring the mass fragments indicative of 1-PA (m/z = 30, 59) via the QMS, an example of which is shown in the accompanying Supporting Information (Figure S4), with exposure to 1-PA maintained for 100 s upon attaining a QMS signal of ∼2 × 10^4 counts for m/z = 30 in all cases. All samples were initially heated via a linear temperature ramp (1 K/s) to 223 K for 300 s as a thermal pretreatment to remove physisorbed 1-PA from the HOPG substrate and then were rapidly cooled to 100 K. The typical desorption profile observed for 1-PA multilayer physidesorption is shown in the accompanying SI (Figure S5). During this pretreatment, the QMS was used to measure the desorption profile of all m/z ratios monitored during the full temperature ramp, with the samples positioned approximately 5 cm away from the inlet aperture to prevent overloading of the SEM detector during the desorption of molecularly adsorbed species. The samples were then positioned to within several millimeters of the inlet aperture and heated via a linear temperature ramp (1 K/s) until reaching a final temperature of 773 K.

https://doi.org/10.1021/acs.jpca.2c03149
J. Phys. Chem. A 2022, 126, 7578−7590

RESULTS AND DISCUSSION

Cluster Ion Mass Analysis and Deposition. Typical mass spectra collected for beams of $Pt_1Zr_xO_y^-$ and $Zr_xO_y^-$ generated by reactive magnetron sputtering are compared in Figure 1.

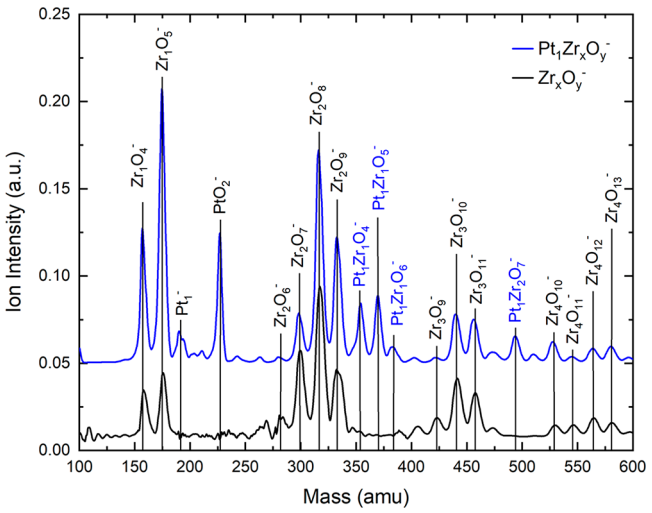

Figure 1. Mass spectra acquired for cluster anion beams generated by magnetron sputtering of Pt/Zr (blue) and Zr (black) targets.

Comparison of the mass spectra acquired for each sputtering target composition allows the confident assignment of Pt-containing clusters to candidate peaks based on the coincidence of their presence in the $Pt_1Zr_xO_y^-$ beam and their absence from the $Zr_xO_y^-$ beam. Moreover, the assigned $Pt_1Zr_xO_y^-$ peaks in Figure 1 clearly show why the $Pt_1Zr_2O_7$ cluster was chosen for these experiments, as it is the most readily attainable cluster stoichiometry in which the Zr content exceeds that of Pt, and this cluster gives a clean peak in the mass spectrum with virtually no overlap with other species.

Ensuring soft-landing conditions is critical in the preparation of supported size-selected cluster samples. If clusters are deposited with excessive kinetic energy, fragmentation of the clusters and surface damage to the substrate become highly likely.[60,61] Hence, for typical cluster beamline conditions, the energy of mass-selected clusters deposited onto a prepared HOPG substrate was determined empirically via retarding field analysis. Assuming one unit of elementary charge per cluster ion, the energy spread of the cluster beam can be calculated by taking the negative first derivative of the measured discharge current as a function of voltage bias applied to the substrate. The result of this analysis is shown in Figure S3 within the Supporting Information. Based on the calculated beam energy distribution shown in Figure S2, virtually all cluster anions impinging on the surface do so with between ~7.3 and 21.3 eV of total energy per cluster, corresponding to an energy range of 0.73−2.13 eV/atom for each cluster. During depositions for preparing supported cluster samples, the HOPG substrate was maintained at approximately −10 V, the maximum bias possible before considerable degradation of the deposition current was observed. This ensured that all deposited cluster ions were well below the 1 eV/atom threshold for soft-landing conditions.

Though great care was taken to ensure that samples of intact, monodispersed clusters were prepared on the HOPG support, it is still possible for clusters to become mobile on the support surface after deposition. This is especially true for substrates where the cluster−support interaction is quite weak, as is known to be the case for HOPG.[62−65] The low temperature of the substrate (100 K) maintained via LN_2-cooling should minimize this phenomenon during cluster deposition and reactant dosing, but the propensity for cluster mobilization and diffusion across the surface will likely increase with increasing surface temperature. Previous work in this laboratory sought to compare the propensities of size-selected metal and metal oxide clusters for diffusion on a defect-free HOPG surface.[59] A comparison of STM imaging done for samples prepared via soft landing at room temperature of exclusively $Mo_{100\pm2.5}^-$ or $(MoO_3)_{67\pm1.5}^-$, these being metallic and metal oxide clusters having the same nominal mass, found that the metallic clusters were preferentially organized along step edges, while the metal oxide clusters were stochastically distributed across terraces. These observations suggest that,

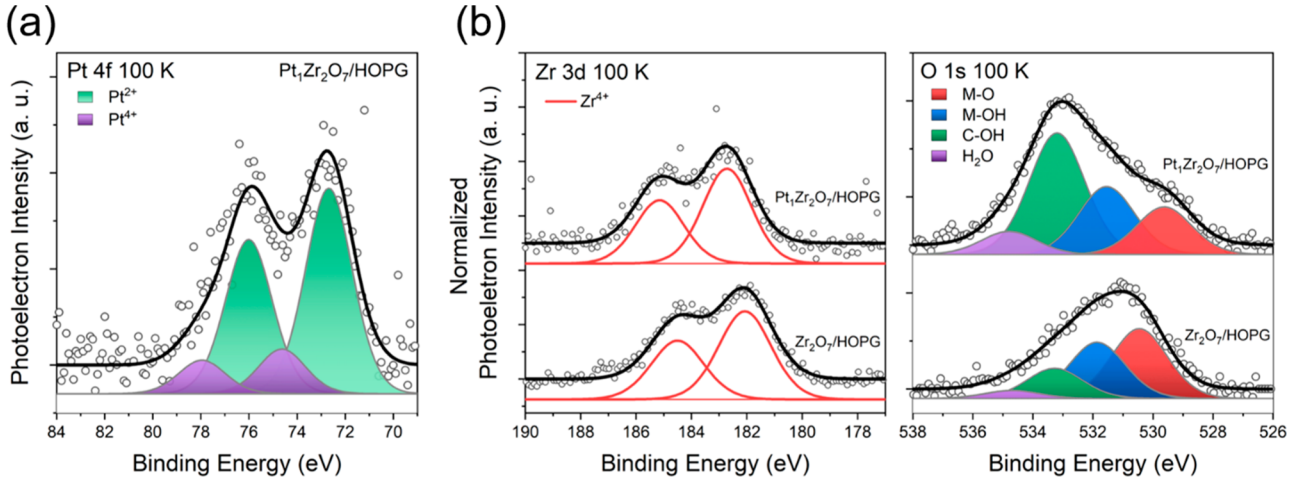

Figure 2. XPS measurements acquired for cluster samples as-prepared in vacuo at 100 K. (a) Pt 4f region for as-prepared $Pt_1Zr_2O_7$/HOPG fitted with spin−orbit doublets corresponding to Pt^{2+} (green) and Pt^{4+} (purple) states. (b) Comparison of Zr 3d and O 1s regions for as-prepared $Pt_1Zr_2O_7$/HOPG and Zr_2O_7/HOPG. The Zr 3d region is fitted with spin−orbit doublets corresponding to the Zr^{4+} state, and the O 1s region is fitted with single peaks corresponding to various oxygen-containing species.

https://doi.org/10.1021/acs.jpca.2c03149
J. Phys. Chem. A 2022, 126, 7578−7590

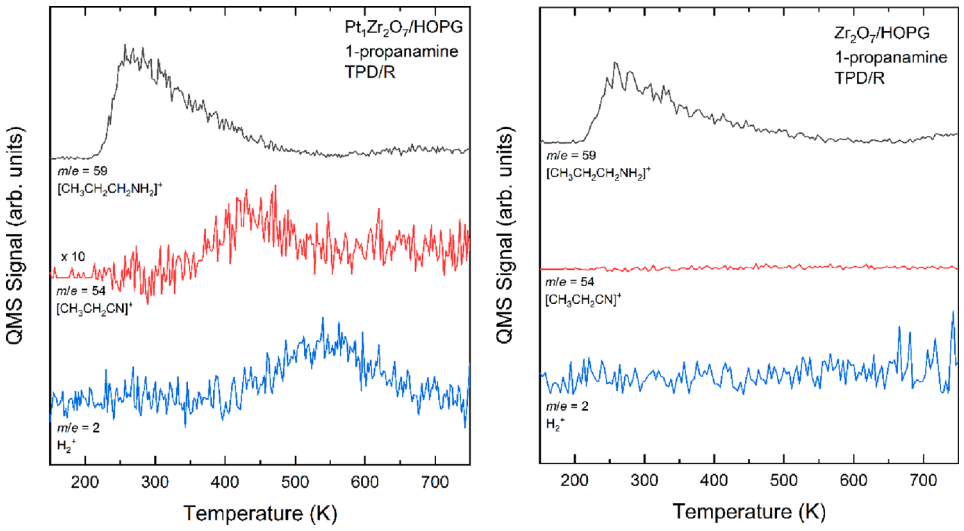

Figure 3. TPD/R spectra acquired for prepared cluster samples exposed to a dose of 1-PA in vacuo at a substrate temperature of 100 K and following initial thermal treatment to 223 K. In both cases, the m/z ratios indicative of 1-PA (59), propionitrile (54), and H_2 (2) are shown. The signal for m/z = 54 has been corrected for contributions because of fragmentation of 1-PA and the signal for m/z = 2 has undergone subtraction of a rising background feature.

although metal clusters appear to diffuse readily across the surface to find more ideal binding sites, metal oxide clusters of similar mass need not feel such inclination.

In another investigation using metal oxide clusters of similar size to the $Pt_1Zr_2O_7$ clusters used here, $(WO_3)_3^-$ clusters were soft-landed at submonolayer coverage onto defect-free HOPG at 100 K and were characterized by ex-situ AFM imaging.[66] After exposure to the atmosphere during sample transfer, the clusters were found to have formed two-dimensional, ramified fractal assemblies, which were stable upon annealing to as high as 673 K. Similar structures have been observed and reported by others for samples prepared by depositing small, mass-selected metal oxide clusters onto relatively inert substrates, such as Au(111), in UHV.[67,68] Therefore, even if the supported clusters become mobilized and diffuse across the surface, there is ample evidence that the clusters may indeed not experience transformative agglomeration, that is to say, a complete loss of the model SAC-active site within the initial clusters. The most important factor to ensure here in this study, is the isolation of single Pt atoms, as opposed to the formation of larger Pt particles, during the initial interaction and reaction with 1-PA.

Characterization of Supported Clusters. After mass selection and deposition of the chosen cluster anion species on the cold HOPG substrate, the resulting supported neutral cluster sample was characterized by XPS. The results of XPS measurements for each of the as-prepared cluster samples are shown in Figure 2.

The Pt 4f spectrum is typical of those acquired for a broad range of Pt SACs prepared on a variety of metal oxide supports.[42] In particular, the observed states are in general agreement with measurements acquired for a Pt_1/ZrO_2 catalyst prepared by Li et al. via atomic layer deposition in their comparison of several synthesized Pt SACs in the room temperature hydrolytic dehydrogenation of ammonia borane to generate H_2.[69] The spectrum here for $Pt_1Zr_2O_7$/HOPG shows that Pt^{2+} is the predominant state for Pt in the prepared cluster samples, with some Pt^{4+} present as well. Integrated areal analysis of the spin−orbit doublets fitted to each state allows for quantitative comparison of the prevalence of each state and gives a ratio of 4.6:1 for the relative amount of Pt^{2+} to Pt^{4+}. Notably, there is no detectable presence of the Pt^0 state, indicating that all the Pt atoms in the sample are oxygen-bound, and there is no feature corresponding to metallic Pt, excluding the presence of Pt nanoparticles[70−73] which could form via cluster fragmentation and subsequent agglomeration in a deposition process.[74−77] This supports the successful soft landing of cluster ions at the substrate surface with low kinetic energies. The Zr 3d spectrum acquired for as-prepared Zr_2O_7/HOPG shows a Zr $3d_{5/2}$ binding energy of 182.1 eV, which is consistent with a Zr^{4+} state.[78−80] By comparison, the Zr $3d_{5/2}$ feature for the $Pt_1Zr_2O_7$/HOPG sample is shifted to a higher binding energy of 182.7 eV, comprising a 0.6 eV binding energy shift. We expect the Pt_1-containing clusters to be structured such that the Pt atom is coordinated to oxygen atoms shared with Zr atoms in the cluster. The Zr 3d data observed here support this prospect, in particular there is no evidence of direct bonding, i.e., alloying, of Pt to Zr, which would produce a lower binding energy shift for the Zr 3d feature.[81]

The O 1s spectra have been fit with a semiempirical peak model resulting from comparison between data spanning multiple supported cluster samples and experiments. The peak model fitted to the O 1s spectrum acquired for as-prepared Zr_2O_7/HOPG suggests the presence of multiple distinguishable oxygen-containing species. The lowest binding energy feature (red) fitted to the O 1s spectrum has a binding energy of 530.4 eV and is attributed to zirconium-bound oxygen, typical of that measured for ZrO_2.[82] The next lowest binding energy feature (blue) fitted has a binding energy of 531.6 eV and is consistent with oxygen in various metal-bound hydroxyl species reported in the literature.[83,84] The two higher binding energy features fitted are the results of the cold substrate surface adsorbing residual oxygen containing species from the vacuum chamber volume. This was determined by a series of control experiments performed for our system which show that these features manifest for clean HOPG after cooling to 100 K in vacuo (Figure S6). The intensity of the features increases with time spent at this temperature and decrease because of molecular desorption as the substrate is heated.

https://doi.org/10.1021/acs.jpca.2c03149
J. Phys. Chem. A 2022, 126, 7578−7590

A similar peak model can be fitted to the O 1s spectrum acquired for as-prepared $Pt_1Zr_2O_7$/HOPG, with some slight differences. The lowest binding energy feature (red) fitted to this spectrum is shifted to a lower binding energy of 529.6 eV, comprising a shift of 0.8 eV relative to the metal oxide O 1s feature for Zr_2O_7/HOPG. This shift is likely because of the presence of Pt-bound oxygen species in the $Pt_1Zr_2O_7$ cluster, as atomic oxygen chemisorbed to Pt single crystal surfaces has been found to exhibit O 1s binding energies less than 530.4 eV.[85] While occurring at the same binding energy as in the Zr_2O_7/HOPG sample, the O 1s feature assigned to metal-bound hydroxyl species has an intensity surpassing that of the metal oxide feature. This suggests that $Pt_1Zr_2O_7$/HOPG has a greater propensity for forming metal hydroxyl species than Zr_2O_7/HOPG does. The two higher binding energy features are more intense for as-prepared $Pt_1Zr_2O_7$/HOPG relative to Zr_2O_7/HOPG, but this is expected in part because of the longer deposition time required because of a lower and less stable mass-selected cluster ion flux for the $Pt_1Zr_2O_7^-$ cluster beam compared with that of the $Zr_2O_7^-$ beam in our experiments. This leaves more time for residual species from the vacuum chamber to adsorb onto the cold substrate.

Cluster Reactivity with 1-PA. The reactivity of $Pt_1Zr_2O_7$/HOPG and Zr_2O_7/HOPG with 1-PA was probed via TPD/R experiments and XPS measurements. The results of the TPD/R experiments for each supported cluster sample are compared in Figure 3.

The TPD/R spectrum acquired for $Pt_1Zr_2O_7$/HOPG exposed to 1-PA shows the desorption of intact 1-PA, along with propionitrile, and H_2. The desorption profile for 1-PA closely matches that observed during a control TPD experiment for clean HOPG exposed to 1-PA (Figure S9). Hence, this desorption feature is largely because of 1-PA molecularly desorbed from the bare regions of the HOPG surface or from the sample holder assembly. The desorption profile for propionitrile is centered at 425 K and has been corrected for contribution because of fragmentation of 1-PA. The desorption profile for H_2 is centered at 550 K and has undergone the subtraction of a rising background feature, which is present in the signal for m/z = 2 in all TPD/R spectra for our system. The raw TPD/R data acquired for $Pt_1Zr_2O_7$/HOPG exposed to 1-PA is shown in the accompanying Supporting Information (Figure S7). The desorption of propionitrile and H_2 are not observed during control TPD experiments for 1-PA on clean HOPG. In a control TPD experiment performed for as-prepared $Pt_1Zr_2O_7$/HOPG without 1-PA exposure (Figure S8), some slight desorption of H_2 is observed at a slightly higher temperature than that observed during the TPD/R experiment. This weak effect can be attributed to the desorption of H_2 resulting from recombination of H atoms from cluster-bound hydroxyl species already present on the clusters, likely because of interaction with adventitious H_2 or H_2O in the UHV system during the time between the beginning of sample preparation (cluster deposition) and performance of the TPD experiment. Some very slight desorption for m/z = 28 is observed during the control TPD experiment, but notably there is no corresponding desorption signal observed for m/z = 54. This feature is attributed to the desorption of adventitious CO, having adsorbed during sample preparation. Given that some contamination of samples by adventitious species within the system had occurred, attempts were made to minimize the time between initiation of cluster deposition and the performance of measurements for given experiments. For this reason, TPD/R and XPS experiments were always performed on separately, but identically, prepared samples. By comparison of the results of these two experiments, it is apparent that the evolution of propionitrile and H_2 stemming from exposure of the $Pt_1Zr_2O_7$ clusters has occurred.

The TPD/R spectrum acquired for Zr_2O_7/HOPG exposed to 1-PA is virtually identical to that of the control TPD experiment for 1-PA exposed to clean HOPG (Figure S9). Not only was there no desorption of propionitrile or H_2 observed, but neither was there desorption of any other obvious oxidative reaction products that was checked for, including propanamide, propionaldehyde, propylene, propane, or combustion products (see Figure S10). Hence, the reactivity observed for $Pt_1Zr_2O_7$/HOPG toward 1-PA seems to be intimately dependent on the presence of the single Pt atom.

To further investigate the nature of the reaction between $Pt_1Zr_2O_7$/HOPG and 1-PA, a series of XPS measurements were acquired immediately following (i) exposure of the as-prepared sample to a dose of 1-PA at 100 K, (ii) thermal pretreatment to 223 K, and (iii) a full TPD/R heating ramp to 773 K. These measurements included the N 1s, C 1s, O 1s, Zr 3d, and Pt 4f core level regions. The spectra acquired for the N 1s region are shown in Figure 4.

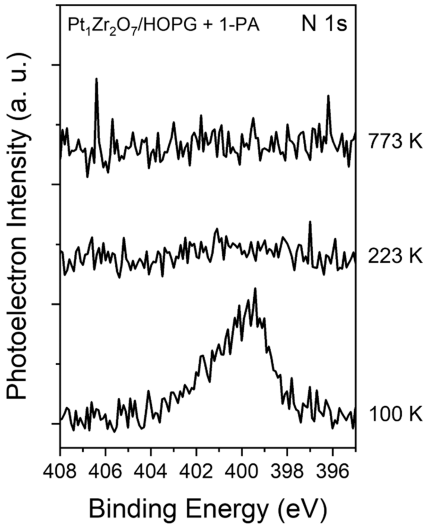

Figure 4. XPS measurements for the N 1s region acquired for as-prepared $Pt_1Zr_2O_7$/HOPG exposed to a dose of 1-PA in vacuo (i) at a substrate temperature of 100 K, and after cooling back to 100 K following (ii) thermal pretreatment at 223 K, and (iii) full TPD/R heating ramp to 773 K.

The feature present after exposing $Pt_1Zr_2O_7$/HOPG to 1-PA at 100 K comprises a slightly asymmetric feature with a peak binding energy at 399.7 eV, which is consistent with adsorbed propylamine and other primary alkylamines.[86,87] After thermal pretreatment and cooling back to 100 K, the N 1s feature has been dramatically reduced, with a hint of signal within the binding energy range spanning 402 to 398 eV. Unfortunately, because of the low surface coverage nature of the prepared cluster sample and the resulting low density of active adsorption sites, coupled with the low relative sensitivity to nitrogen in XPS measurements, we are unable to extract more useful information about any surface-bound N-containing species for the present system. Moreover, based on the overall

https://doi.org/10.1021/acs.jpca.2c03149
J. Phys. Chem. A 2022, 126, 7578−7590

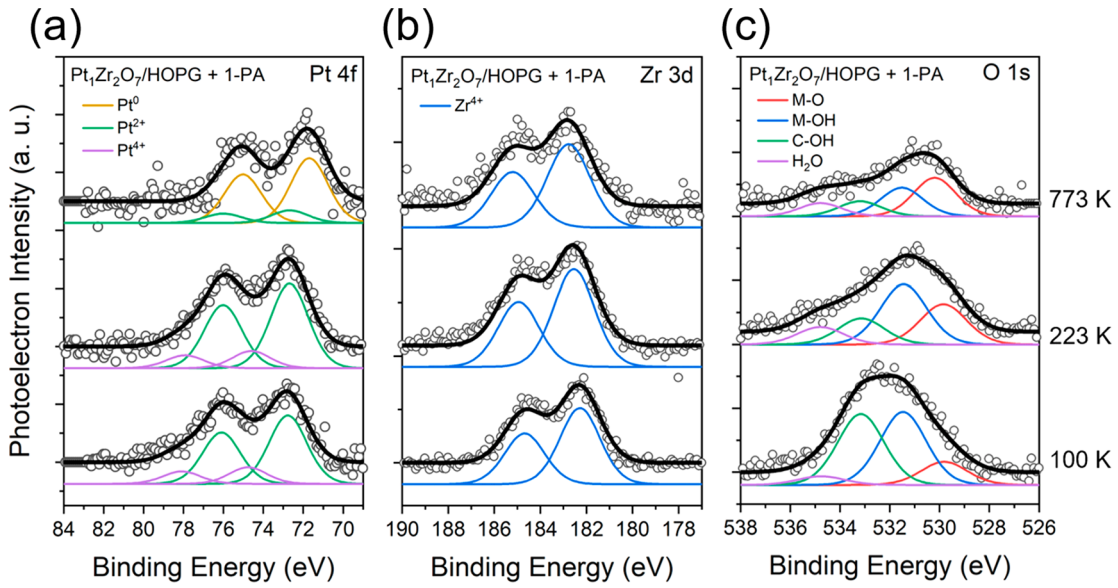

Figure 5. XPS measurements acquired for as-prepared $Pt_1Zr_2O_7$/HOPG exposed to a dose of 1-PA in vacuo (i) at a substrate temperature of 100 K, and after cooling back to 100 K and following (ii) thermal pretreatment at 223 K and (iii) a full TPD/R heating ramp to 773 K. (a) Pt 4f region fitted with spin−orbit doublets corresponding to Pt^0 (yellow), Pt^{2+} (green), and Pt^{4+} (purple) states. (b) Zr 3d region fitted with a spin−orbit doublet corresponding to the Zr^{4+} state. (c) O 1s region fitted with singlet peaks corresponding to various oxygen-containing species.

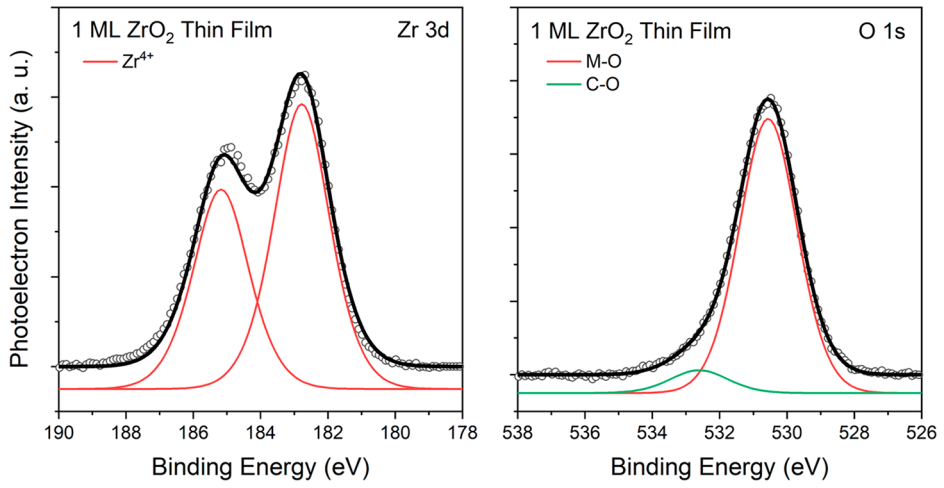

Figure 6. XPS measurements acquired for an as-prepared ZrO_{2+x}/HOPG sample at a substrate temperature of 298 K. (a) Zr 3d region fitted with a spin−orbit doublet corresponding to the Zr^{4+} state. (b) O 1s region fitted with singlet peaks corresponding to a metal-bound oxygen and organic-bound oxygen.

signal measured for the Pt 4f region for our samples, even if 1-PA was present at a ratio of 1 molecule per cluster, the expected N 1s signal would be hardly above baseline detection limits within our system. Furthermore, the C 1s signal arising from the HOPG substrate overwhelms any signal present because of carbon in adsorbed organic species like 1-PA or any surface-bound intermediates at such low coverage, making further direct identification impossible.

The corresponding spectra acquired for the Pt 4f, Zr 3d, and O 1s regions for are shown in Figure 5.

Comparison between the Pt 4f and Zr 3d regions for the as-prepared $Pt_1Zr_2O_7$/HOPG and following exposure to 1-PA at 100 K shows no discernible difference for the Pt states present but does exhibit a 0.4 eV shift toward lower binding energy for the Zr $3d_{5/2}$ peak. This suggests the binding of 1-PA to a Zr atom in the cluster, which is known to occur via the nitrogen lone pair for a number of amines on metal and metal oxide surfaces.[88−90] In the O 1s spectra, the amount of signal arising from metal hydroxyl species relative to that arising from metal oxide species after exposure to 1-PA and subsequent thermal pretreatment, is greater than that for pretreated $Pt_1Zr_2O_7$/HOPG without 1-PA exposure by ∼25%. This suggests the presence of additional hydroxyl groups after exposure to 1-PA and heating to 223 K, indicating at least some dehydrogenation beginning to occur at fairly low temperature. After a full TPD/R temperature ramp, the total signal for metal hydroxyls has decreased to below that of the metal oxide oxygen. This agrees with the observed liberation of H_2 in the TPD/R experiments embodied by the H_2 desorption feature. After the full temperature ramp, the Zr 3d spectrum remains largely unchanged, which agrees with the reported high-temperature stability observed for various forms of ZrO_2.[91] The Pt 4f spectrum, however, shows a fairly dramatic change, with the complete disappearance of the Pt^{4+} state, as well as the

https://doi.org/10.1021/acs.jpca.2c03149
J. Phys. Chem. A 2022, 126, 7578−7590

diminution of the Pt^{2+} state and the appearance of a dominant feature at 71.7 eV, typical of a Pt^0 state for very small forms of Pt.[92]

ZrO_{2+x} Ultrathin Film Reactivity with 1-PA. In order to further investigate whether the lack of observed reactivity toward 1-PA for Zr_2O_7/HOPG stemmed from the small size of the monodisperse Zr_2O_7 clusters, an additional experiment was performed involving a substantially higher loading of overly oxidized Zr. A non-mass-selected beam of Zr_xO_y cluster anions was deposited onto a clean HOPG substrate at 298 K with no retarding voltage, allowing the deposited clusters a greater chance for mobility on the substrate surface. The goal of this deposition procedure was to form an amorphous zirconium oxide sample, with the same overly oxidized nature as the Zr_2O_7 clusters, but without the monodispersed character of Zr_2O_7/HOPG. XPS measurements acquired for the prepared ZrO_{2+x}/HOPG sample are shown in Figure 6.

The Zr 3d region was fitted with a single spin−orbit doublet with a Zr $3d_{5/2}$ binding energy of 182.8 eV, in very good agreement with other ZrO_2 thin film results reported in the literature.[91] The O 1s region was fitted with two distinct singlet peaks to account for the observed slight asymmetry of the feature, with a dominant singlet at 530.5 eV, assigned to the oxygen bound to Zr, and a weak feature at 532.6 eV, assigned to the oxygen bound to carbon in HOPG. Moreover, integrated areal analysis of these spectra confirmed that the sample was excessively oxidized, with a calculated O:Zr relative atomic ratio of 2.5:1, after accounting for the relative sensitivity to each element.[93]

A TPD/R experiment was also performed for the prepared ZrO_{2+x} ultrathin film following exposure to 1-PA at 100 K. The results of this experiment are shown in Figure 7.

The TPD/R spectrum acquired for ZrO_{2+x}/HOPG highly resembles that of Zr_2O_7/HOPG. There is no clear feature indicative of propionitrile or H_2 desorption, and no evidence was observed for any other oxidation products that were checked for (see Figure S11). Hence, excessively oxidized zirconium in both monodisperse small cluster form and an amorphous ultrathin film form appear to be unreactive toward 1-PA.

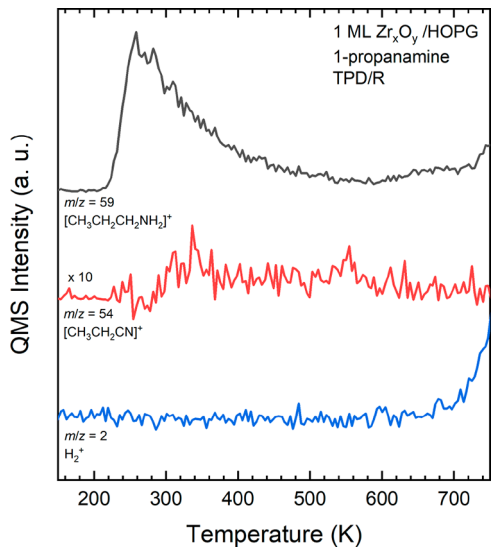

Figure 7. TPD/R spectra acquired for ZrO_{2+x}/HOPG exposed to 1-PA in vacuo at a substrate temperature of 100 K and following thermal pretreatment to 223 K. The m/z ratios indicative of 1-PA, propionitrile, and H_2 are shown. The signal for m/z = 54 has been corrected because of fragmentation of 1-PA.

Though there has not been much investigation into the propensity for ZrO_2 to facilitate the selective dehydrogenation of primary alkylamines to nitriles and H_2, aside from early work demonstrating this ability[47] and the recent report by Gorte et al.,[38] extensive work has been done to reveal the nature of light alkane dehydrogenation over ZrO_2 in various forms. Very compelling experimental studies reported by Otroshchenko et al. strongly evidenced the critical role of coordinatively unsaturated Zr^{4+} cations associated with oxygen vacancies as the active site for dehydrogenating several light alkanes, including propane, isobutane, and *n*-butane.[94,95] Moreover, it was shown that the inclusion of promoter metal oxide species into the bulk of the ZrO_2 catalysts facilitated an increased concentration of oxygen vacancies, which was directly correlated to an increase in dehydrogenation activity.[96] This phenomenon has been observed by others as well, for example, in the promotion of coordinatively unsaturated Zr^{4+} defect density driving an increase in propane dehydrogenation activity.[97] High-temperature reduction treatments were necessary to induce the formation of vacancy sites, which showed marked improvements in catalytic performance over their fully oxidized counterparts. In separate work reported by Zhang et al., it was similarly demonstrated that the cations of oxygen vacancy sites play a crucial role in dehydrogenation activity for nanosized ZrO_2 crystallites, with their increasing concentration on smaller crystallites driving an increase in activity upon reducing the size of the crystallites from 43 to 1 nm.[98,99] It is reasonable to expect that such active sites are likely responsible for the dehydrogenation of 1-propanamine observed on bulk samples of ZrO_2 as well. This would seem to agree well with the results reported here, as both the monodisperse Zr_2O_7 clusters and ZrO_{2+x} ultrathin film constitute samples that are severely deficient in the critical oxygen vacancies.

CONCLUSION

The application of surface supported, mass-selected cluster soft landing in preparing model SAC active sites was reported here for the first time. This was accomplished through the use of a newly constructed cluster ion beamline and surface analytical apparatus. The combination of mass spectrometry and mass-selection predeposition and XPS characterization postdeposition confirmed the successful soft landing of $Pt_1Zr_2O_7^-$ cluster anions onto a prepared HOPG substrate, resulting in a monodispersed $Pt_1Zr_2O_7$/HOPG model SAC system. The reactivity of this system toward a model functionalized hydrocarbon molecule, 1-PA, was investigated via TPD/R and XPS measurements. It was shown that the $Pt_1Zr_2O_7$ cluster successfully reacted with 1-PA to exclusively form propionitrile and H_2, which are the optimal reaction products for endothermic fuel applications. By comparison with Zr_2O_7/HOPG, it was shown that the observed reactivity for $Pt_1Zr_2O_7$/HOPG is critically dependent on the presence of the Pt atom, as its absence results in a complete loss of activity. Moreover, it was shown through comparison with an overoxidized ZrO_{2+x} ultrathin film that the inactivity of Zr_2O_7/HOPG likely results from a lack of oxygen vacancy sites, rather than the monodisperse nature of the Zr_2O_7 clusters.

https://doi.org/10.1021/acs.jpca.2c03149
J. Phys. Chem. A 2022, 126, 7578−7590

■ ASSOCIATED CONTENT

Supporting Information

The Supporting Information is available free of charge at https://pubs.acs.org/doi/10.1021/acs.jpca.2c03149.

Detailed apparatus description, retarding field analysis of cluster anion beam, XPS of clean HOPG, mass spectra for 1-PA dose profile, 1-PA TPD spectrum acquired during thermal pretreatment, tables of XPS spectra peak fitting values, O 1s XPS measurements for cold HOPG in vacuo, HOPG blank TPD measurements for bare substrate and after 1-PA exposure, raw TPD/R data for $Pt_1Zr_2O_7$/HOPG, Zr_2O_7/HOPG, and 1 ML ZrO_{2+x}/HOPG exposed to 1-PA (PDF)

■ AUTHOR INFORMATION

Corresponding Author

Kit H. Bowen − *Department of Chemistry, Johns Hopkins University, Baltimore, Maryland 21218, United States;* orcid.org/0000-0002-2858-6352; Email: kbowen@jhu.edu

Authors

Michael A. Denchy − *Department of Chemistry, Johns Hopkins University, Baltimore, Maryland 21218, United States;* orcid.org/0000-0002-2757-8705

Linjie Wang − *Department of Chemistry, Johns Hopkins University, Baltimore, Maryland 21218, United States;* orcid.org/0000-0002-6558-1753

Benjamin R. Bilik − *Department of Chemistry, Johns Hopkins University, Baltimore, Maryland 21218, United States*

Lucas Hansen − *Department of Chemistry, Johns Hopkins University, Baltimore, Maryland 21218, United States*

Sandra Albornoz − *Department of Chemistry, Johns Hopkins University, Baltimore, Maryland 21218, United States*

Francisco Lizano − *Department of Chemistry, Johns Hopkins University, Baltimore, Maryland 21218, United States*

Nicolas Blando − *Department of Chemistry, Johns Hopkins University, Baltimore, Maryland 21218, United States*

Zachary Hicks − *Department of Chemistry, Johns Hopkins University, Baltimore, Maryland 21218, United States*

Gerd Gantefoer − *Fachbereich fuer Physik, Universitaet Konstanz, 78457 Konstanz, Germany*

Complete contact information is available at: https://pubs.acs.org/10.1021/acs.jpca.2c03149

Notes

The authors declare no competing financial interest.

■ ACKNOWLEDGMENTS

This material is based upon work supported by the Air Force Office of Scientific Research (AFOSR) under Grant Number FA9550-19-1-0077 (KHB).

■ REFERENCES

(1) Kappenstein, C. J.; Batonneau, Y.; Brahmi, R.; Pirault-Roy, L. Propulsion and Catalysis − Historical Survey, Up-to-Date Overview, and Current Challenges. *Int. J. Energetic Mater. Chem. Propulsion* **2010**, *9* (5), 413−436.

(2) Dinda, S.; Vuchuru, K.; Konda, S.; Uttravalli, A. N. Heat Management in Supersonic/Hypersonic Vehicles Using Endothermic Fuel: Perspective and Challenges. *ACS Omega* **2021**, *6* (40), 26741−26755.

(3) Lander, H.; Nixon, A. C. Endothermic Fuels for Hypersonic Vehicles. *J. Aircraft* **1971**, *8* (4), 200−207.

(4) Huang, H.; Spadaccini, L. J.; Sobel, D. R. Fuel-cooled thermal management for advanced aeroengines. *J. Eng. For Gas Turbines and Power* **2004**, *126* (2), 284−293.

(5) Ning, W.; Yu, P.; Jin, Z. Research status of active cooling of endothermic hydrocarbon fueled scramjet engine. *Proc. Inst. Mech. Eng., Pt. G: J. Aerospace Engineering* **2012**, *2227* (11), 1780−1794.

(6) Hubesch, R.; Mazur, M.; Foger, K.; Selvakannan, P. R.; Bhargava, S. Zeolites on 3D-printed open metal framework structure: metal migration into zeolite promoted catalytic cracking of endothermic fuels for flight vehicles. *Chem. Commun.* **2021**, *57*, 9586−9589.

(7) Yeh, Yu-Hao; Yu, J.; Luo, J.; Gorte, R. J. Endothermic Reforming of *n*-Hexanes on Metal (Pt, Ga) Containing H-ZSM-5 at High Pressures. *Ind. Eng. Chem. Res.* **2015**, *54* (43), 10675−10683.

(8) Horn, R.; Schlogl, R. Methane Activation by Heterogeneous Catalysis. *Catal. Lett.* **2015**, *145*, 23−39.

(9) Coperet, C. C−H Bond Activation and Organometallic Intermediates on Isolated Metal Centers on Oxide Surfaces. *Chem. Rev.* **2010**, *110*, 656−680.

(10) Atkins, M. P.; Evans, G. R. Catalytic dehydrogenation − a review of current processes and innovations. *Erdöl Erdgas Kohle* **1995**, *111* (6), 271−274.

(11) Vora, B. V. Development of Dehydrogenation Catalysts and Processes. *Top. Catal.* **2012**, *55*, 1297−1308.

(12) Kumar, M. S.; Chen, D.; Walmsley, J. C.; Holmen, A. Dehydrogenation of Propane over Pt-SBA-15: Effect of Pt Particle Size. *Catal. Commun.* **2008**, *9* (5), 747−750.

(13) Xie, C.; Yan, D.; Li, H.; Du, S.; Chen, W.; Wang, Y.; Zou, Y.; Chen, R.; Wang, S. Defect Chemistry in Heterogeneous Catalysis: Recognition, Understanding, and Utilization. *ACS Catal.* **2020**, *10*, 11082−11098.

(14) Liu, Z.-P.; Hu, P. General Rules for Predicting Where a Catalytic Reaction Should Occur on Metal Surfaces: A Density Functional Theory Study of C − H and C − O Bond Breaking/Making on Flat, Stepped, and Kinked Metal Surfaces. *J. Am. Chem. Soc.* **2003**, *125*, 1958−1967.

(15) Boller, B.; Durner, K. M.; Wintterlin, J. The Active Sites of a Working Fischer−Tropsch Catalyst Revealed by Operando Scanning Tunneling Microscopy. *Nat. Catal.* **2019**, *2*, 1027−1034.

(16) Zhu, J.; Yang, M.-L.; Yu, Y.; Zhu, Y.-A.; Sui, Z.-J.; Zhou, X.-G.; Holmen, A.; Chen, D. Size-Dependent Reaction Mechanism and Kinetics for Propane Dehydrogenation over Pt Catalysts. *ACS Catal.* **2015**, *5*, 6310−6319.

(17) Yang, M.-L.; Zhu, J.; Zhu, Y.-A.; Sui, Z.-J.; Yu, Y.-D.; Zhou, X.-G.; Chen, D. Tuning selectivity and stability in propane dehydrogenation by shaping Pt particles: A combined experimental and DFT study. *J. Mol. Catal. A* **2014**, *395*, 329−336.

(18) Lian, Z.; Si, C.; Jan, F.; Zhi, S.; Li, B. Coke Deposition on Pt-Based Catalysts in Propane Direct Dehydrogenation: Kinetics, Suppression, and Elimination. *ACS Catal.* **2021**, *11*, 9279−9292.

(19) Siddiqi, G.; Sun, P.; Galvita, V.; Bell, A. T. Catalyst performance of novel Pt/Mg(Ga)(Al)O catalysts for alkane dehydrogenation. *J. Catal.* **2010**, *274*, 200−206.

(20) Huang, H.; Spadaccini, L. J. Coke Removal in Fuel-Cooled Thermal Management Systems. *Ind. Eng. Chem. Res.* **2005**, *44*, 267−278.

(21) Li, S.; Zhang, B.; Liu, G. Metal-based catalysts for the non-oxidative dehydrogenation of light alkanes to light olefins. *React. Chem. Eng.* **2021**, *6*, 9−26.

(22) Zaera, F.; Chrysostomou, D. Propylene on Pt(111) II. Hydrogenation, dehydrogenation, and H−D exchange. *Surf. Sci.* **2000**, *457*, 89−108.

(23) Fearon, J.; Watson, G. W. Hydrogen adsorption and diffusion on Pt {111} and PtSn {111}. *J. Mater. Chem.* **2006**, *16*, 1989−1996.

(24) Lieske, H.; Sarkany, A.; Volter, J. Hydrocarbon Adsorption and Coke Formation on Pt/Al_2O_3 and $Pt-Sn/Al_2O_3$ Catalysts. *Appl. Catal.* **1987**, *30*, 69−80.

(25) Cortright, R. D.; Hill, J. M.; Dumesic, J. A. Selective dehydrogenation of isobutane over supported Pt/Sn catalysts. *Catal. Today* **2000**, *55*, 213−223.
(26) Cortright, R. D.; Dumesic, J. A. Microcalorimetric, Spectroscopic, and Kinetic Studies of Silica-Supported Pt and Pt/Sn Catalysts for Isobutane Dehydrogenation. *J. Catal.* **1994**, *148*, 771−778.
(27) Baxter, E. T.; Ha, M.-A.; Cass, A. C.; Alexandrova, A. N.; Anderson, S. L. Ethylene Dehydrogenation on $Pt_{4,7,8}$ Clusters on Al_2O_3: Strong Cluster Size Dependence Linked to Preferred Catalyst Morphologies. *ACS Catal.* **2017**, *7*, 3322−3335.
(28) Ding, X.; Zhu, H.; Ren, H.; Liu, D.; Yu, Z.; Shi, N.; Guo, W. Adsorption and dehydrogenation of C_2−C_6 *n*-alkanes over a Pt catalyst: a theoretical study on the size effects of alkane molecules and Pt substrates. *Phys. Chem. Chem. Phys.* **2020**, *22*, 21835−21843.
(29) Jablonski, E. L.; Castro, A. A.; Scelza, O. A.; Miguel, S. R. Effect of Ga addition to Pt/Al_2O_3 on the activity, selectivity and deactivation in the propane dehydrogenation. *Appl. Catal. A: General* **1999**, *183*, 189−198.
(30) Wang, X.; Yang, D.; Xu, Yong; Zhong, J.; Zhang, Q. Colloidal synthesis of Pt−In bimetallic nanoparticles for propane dehydrogenation. *Can. J. Chem.* **2017**, *95*, 1135−1140.
(31) Ballarini, A. D.; Miguel, S. R.; Castro, A. A.; Scelza, O. A. n-Decane dehydrogenation on Pt, PtSn and PtGe supported on spinels prepared by different methods of synthesis. *Appl. Catal. A.: General* **2013**, *467*, 235−245.
(32) Nagaraja, B. M.; Shin, C.-H.; Jung, K.-D. Selective and stable bimetallic $PtSn/\theta$-Al_2O_3 catalyst for dehydrogenation of *n*-butane to *n*-butenes. *Appl. Catal. A.: General* **2013**, *467*, 211−223.
(33) Siri, G. J.; Ramallo-Lopez, J. M.; Casella, M. L.; Fierro, J. L. G.; Requejo, F. G.; Ferretti, O. A. XPS and EXAFS study of supported PtSn catalysts obtained by surface organometallic chemistry on metals Application to the isobutane dehydrogenation. *Appl. Catal. A.: General* **2005**, *278*, 239−249.
(34) Ha, M.-A.; Baxter, E. T.; Cass, A. C.; Anderson, S. L. Boron Switch for Selectivity of Catalytic Dehydrogenation on Size-Selected Pt Clusters on Al_2O_3. *J. Am. Chem. Soc.* **2017**, *139*, 11568−11575.
(35) Gorey, T. J.; Zandkarimi, B.; Li, G.; Baxter, E. T.; Alexandrova, A. N.; Anderson, S. L. Preparation of Size- and Composition-Controlled Pt_nSn_x/SiO_2 (n = 4, 7, 24) Bimetallic Model Catalysts with Atomic Layer Deposition. *J. Phys. Chem. C* **2019**, *123*, 16194−16209.
(36) Li, G.; Zandkarimi, B.; Cass, A. C.; Gorey, T. J.; Allen, B. J.; Alexandrova, A. N.; Anderson, S. L. Sn-modification of Pt7/alumina model catalysts: Suppression of carbon deposition and enhanced thermal stability. *J. Chem. Phys.* **2020**, *152* (2), No. 024702.
(37) Gorey, T. J.; Zandkarimi, B.; Li, G.; Baxter, E. T.; Alexandrova, A. N.; Anderson, S. L. Coking-Resistant Sub-Nano Dehydrogenation Catalysts: Pt_nSn_x/SiO_2 (n = 4, 7). *ACS Catal.* **2020**, *10*, 4543−4558.
(38) Cao, T.; Huang, R.; Gorte, R. J.; Vohs, J. M. Endothermic reactions of 1-propanamine on a zirconia catalyst. *Appl. Catal. A: General* **2020**, *590*, 117372.
(39) Shayeghi, A.; Krahling, S.; Hortz, P.; Johnston, R. L.; Heard, C. J.; Schafer, R. Adsorption of Acetonitrile, Benzene, and Benzonitrile on Pt(111): Single Crystal Adsorption Calorimetry and Density Functional Theory. *J. Phys. Chem. C* **2017**, *121* (39), 21354−21363.
(40) Qiao, B.; Wang, A.; Yang, X.; Allard, L. F.; Jiang, Z.; Cui, Y.; Liu, J.; Li, J.; Zhang, T. Single-atom catalysis of CO oxidation using Pt_1/FeO_x. *Nat. Chem.* **2011**, *3*, 634−641.
(41) Yang, X.-F.; Wang, A.; Qiao, B.; Li, J.; Liu, J.; Zhang, T. Single-Atom Catalysts: A New Frontier in Heterogeneous Catalysis. *Acc. Chem. Res.* **2013**, *46* (8), 1740−1748.
(42) Kottwitz, M.; Li, Y.; Wang, H.; Frenkel, A. I.; Nuzzo, R. G. Single Atom Catalysts: A Review of Characterization Methods. *Chemistry-Methods* **2021**, *1* (6), 278−294.
(43) Martin, N.; Cirujano, F. G. Supported Single Atom Catalysts for C−H Activation: Selective C−H Oxidations, Dehydrogenations and Oxidative C−H/C−H Couplings. *ChemCatChem.* **2021**, *13* (12), 2751−2765.
(44) Bruix, A.; Lykhach, Y.; Matolinova, I.; Neitzel, A.; Skala, T.; Tsud, N.; Vorokhta, M.; Stetsovych, V.; Sevcikova, K.; Myslivecek, J.; et al. Maximum Noble-Metal Efficiency in Catalytic Materials: Atomically Dispersed Surface Platinum. *Angew. Chem., Int. Ed.* **2014**, *53*, 10525−105350.
(45) Thomas, J. M. Heterogeneous catalysis: Enigmas, illusions, challenges, realities, and emergent strategies of design. *J. Chem. Phys.* **2008**, *128*, 182502.
(46) Zhang, W.; Wang, H.; Jiang, J.; Sui, Z.; Zhu, Y.; Chen, D.; Zhou, X. Size Dependence of Pt Catalysts for Propane Dehydrogenation: from Atomically Dispersed to Nanoparticles. *ACS Catal.* **2020**, *10*, 12932−12942.
(47) Xu, B.-Q.; Yamaguchi, T.; Tanabe, K. Selective Dehydrogenation of Alkylamines to Nitriles over Metal Oxide Catalysts. *Chem. Lett.* **1988**, *17* (2), 281−284.
(48) Xu, B.-Q.; Yamaguchi, T.; Tanabe, K. Acid-base bifunctional catalysis in the decomposition of alkylamines. *Appl. Catal.* **1991**, *75*, 75−86.
(49) Bernales, V.; Yang, D.; Yu, J.; Gumuslu, G.; Cramer, C. J.; Gates, B. C.; Gagliardi, L. Molecular Rhodium Complexes Supported on the Metal-Oxide-Like Nodes of Metal Organic Frameworks and on Zeolite HY: Catalysts for Ethylene Hydrogenation and Dimerization. *ACS Appl. Mater. Interfaces* **2017**, *9* (39), 33511−33520.
(50) Abdel-Mageed, A. M.; Rungtaweevoranit, B.; Parlinska-Wojtan, M.; Pei, X.; Yaghi, O. M.; Behm, R. J. Highly Active and Stable Single-Atom Cu Catalysts Supported by a Metal-Organic Framework. *J. Am. Chem. Soc.* **2019**, *141*, 5201−5210.
(51) Van Velthoven, N.; Waitschat, S.; Chavan, S. M.; Liu, P.; Smolders, S.; Vercammen, J.; Bueken, B.; Bals, S.; Lillerud, K. P.; Stock, N.; De Vos, D. E. Single-site metal-organic framework catalysts for the oxidative coupling of arenes via C-H/C-H activation. *Chem. Sci.* **2019**, *10* (12), 3616−3622.
(52) Otake, K.; Cui, Y.; Buru, C. T.; Li, Z.; Hupp, J. T.; Farha, O. K. Single-Atom-Based Vanadium Oxide Catalysts Supported on Metal-Organic Frameworks: Selective Alcohol Oxidation and Structure-Activity Relationship. *J. Am. Chem. Soc.* **2018**, *140*, 8652−8656.
(53) Mandal, M.; Cramer, C. J.; Truhlar, D. G.; Sauer, J.; Gagliardi, L. Structure and Reactivity of Single-Site Vanadium Catalysts Supported on Metal-Organic Frameworks. *ACS Catal.* **2020**, *10* (17), 10051−10059.
(54) Ma, X.; Liu, H.; Mao, G.; Zheng, L.; Jiang, H.-L. Modulating Coordination Environment of Single-Atom Catalysts and Their Proximity to Photosensitive Units for Boosting MOF Photocatalysis. *J. Am. Chem. Soc.* **2021**, *143* (31), 12220−12229.
(55) Hoa, L. T.; Nhi, L. T. T.; Son, L. V. T.; Linh, N. L. M.; Hai, H. V. M.; Khieu, D. Q. Single-Atom Ni Heterogeneous Catalysts Supported UiO-66 Structure: Synthesis and Catalytic Activities. *J. Nanomater.* **2021**, *2021*, 1−16.
(56) Wang, L.; Blando, N.; Hicks, Z.; Denchy, M.; Tang, X.; Bluel, H.; Zhang, M.; Gantefor; Bowen, K. H. Combined TPD and XPS Study of Ligation and Decomposition of 1,6-Hexanedithiol on Size-Selected Copper Clusters Supported on HOPG. *J. Phys. Chem. C* **2018**, *122* (4), 2173−2183.
(57) Wang, L.; Denchy, M.; Blando, N.; Hansen, L.; Bilik, B.; Tang, X.; Hicks, Z.; Bowen, K. H. Thermal Decomposition of Dimethyl Methylphosphonate on Size-Selected Clusters: A Comparative Study between Copper Metal and Cupric Oxide Clusters. *J. Phys. Chem. C* **2021**, *125* (21), 11348−11358.
(58) Denchy, M. A.; Wang, L.; Blando, N.; Hansen, L.; Bilik, B. R.; Tang, X.; Hicks, Z.; Gantefoer, G.; Bowen, K. H. Adsorption and Decomposition of Dimethyl Methylphosphonate on Size-Selected Zirconium Oxide Trimer Clusters. *J. Phys. Chem. C* **2021**, *125* (43), 23688−23698.
(59) Wepasnick, K. A.; Li, X.; Mangler, T.; Noessner, S.; Wolke, C.; Grossman, M.; Gantefoer, G.; Fairbrother, D. H.; Bowen, K. H. Surface Morphologies of Size-Selected $Mo_{100\pm2.5}$ and $(MoO_3)_{67\pm1.5}$ Clusters Soft-Landed onto HOPG. *J. Phys. Chem. C* **2011**, *115* (25), 12299−12307.

https://doi.org/10.1021/acs.jpca.2c03149
J. Phys. Chem. A 2022, 126, 7578−7590

(60) Massobrio, C. Molecular Dynamics Study of the Energetic Impact of Ag_{19} on Pd(100): An Interpretation of Mass-Selected Clusters Deposition Experiments. *J. Phys. Chem. B* **1998**, *102*, 4374−4379.
(61) Neuendorf, R.; Palmer, R. E.; Smith, R. Low energy deposition of size-selected Si clusters onto graphite. *Chem. Phys. Lett.* **2001**, *333*, 304−307.
(62) Klett, J.; Krahling, S.; Elger, B.; Schafer, R.; Kaiser, B.; Jaegermann, W. The Electronic Interaction of Pt-Clusters with ITO and HOPG Surfaces upon Water Adsorption. *Z. Phys. Chem.* **2014**, *228* (4−5), 503−520.
(63) Ma, Q.; Rosenberg, R. A. Interaction of A1 clusters with the (0001) surface of highly oriented pyrolytic graphite. *Surf. Sci.* **1997**, *391*, L1224−L1229.
(64) Ma, Q.; Rosenberg, R. A. Interaction of Ti with the (0001) surface of highly oriented pyrolytic graphite. *Phys. Rev. B* **1999**, *60*, 2827.
(65) Muller, U.; Sattler, K.; Xhie, J.; Venkateswaran, N.; Raina, G. A scanning tunneling microscope study of single platinum atoms, platinum dimers and trimers on highly-oriented pyrolytic graphite. *Z. Phys. D − Atoms Molecules Clusters* **1991**, *19* (1-4), 319−321.
(66) Tang, X.; Bowen, K. H.; Calvo, F. Self-assembly of $(WO_3)_3$ clusters on a highly oriented pyrolytic graphite surface and nanowire formation: a combined experimental and theoretical study. *Phys. Chem. Chem. Phys.* **2017**, *19*, 31168−31176.
(67) Goodman, K. R.; Wang, J.; Ma, Y.; Tong, X.; Stacchiola, D. J.; White, M. G. Morphology and reactivity of size-selected titanium oxide nanoclusters on Au(111). *J. Chem. Phys.* **2020**, *152*, No. 054714.
(68) Wang, J.; Ma, Y.; Mahapatra, M.; Kang, J.; Senanayake, S. D.; Tong, X.; Stacchiola, D. J.; White, M. G. Surface structure of mass-selected niobium oxide nanoclusters on Au(111). *Nanotechnolgy* **2021**, *32*, 475601.
(69) Li, J.; Guan, Q.; Wu, H.; Liu, W.; Lin, Y.; Sun, Z.; Ye, X.; Zheng, X.; Pan, H.; Zhu, J.; et al. Highly Active and Stable Metal Single-Atom Catalysts Achieved by Strong Electronic Metal−Support Interactions. *J. Am. Chem. Soc.* **2019**, *141*, 14515−14519.
(70) Mayavan, S.; Sim, J.-B.; Choi, S.-M. Simultaneous reduction, exfoliation and functionalization of graphite oxide into a graphene-platinum nanoparticle hybrid for methanol oxidation. *J. Mater. Chem.* **2012**, *22*, 6953−6958.
(71) Ono, L. K.; Yuan, B.; Heinrich, H.; Cuenya, B. R. Formation and Thermal Stability of Platinum Oxides on Size-Selected Platinum Nanoparticles: Support Effects. *J. Phys. Chem. C* **2010**, *114*, 22119−22133.
(72) Yang, D.-Q.; Zhang, G.-X.; Sacher, E.; Jose-Yacaman, M.; Elizondo, N. Evidence of the Interaction of Evaporated Pt Nanoparticles with Variously Treated Surfaces of Highly Oriented Pyrolytic Graphite. *J. Phys. Chem. B* **2006**, *110*, 8348−8356.
(73) Wertheim, G. K. Shape of core-electron photoemission spectra from metals. *Phys. Rev. B* **1982**, *25*, 1987.
(74) Koizumi, K.; Nobusada, K.; Boero, M. Simple but Efficient Method for Inhibiting Sintering and Aggregation of Catalytic Pt Nanoclusters on Metal-Oxide Supports. *Chem.—Eur. J.* **2017**, *23*, 1531−1538.
(75) Ma, S.; Huang, Z.; Qu, B.; Li, D.; Zhou, R. Coverage-dependent structure and reactivity of vanadia clusters supported on anatase TiO_2(101) surface. *Appl. Surf. Sci.* **2021**, *543*, 148774.
(76) Winans, R. E.; Vajda, S.; Lee, B.; Riley, S. J.; Seifert, S.; Tikhonov, G. Y.; Tomczyk, N. A. Thermal Stability of Supported Platinum Clusters Studied by in Situ GISAXS. *J. Phys. Chem. B* **2004**, *108* (47), 18105−18107.
(77) Brechignac, C.; Cahuzac, Ph.; Carlier, F.; Colliex, C.; Frutos, M.; Kebaili, N.; Le Roux, J.; Masson, A.; Yoon, B. Control of island morphology by dynamic coalescence of soft-landed clusters. *Eur. Phys. J. D* **2001**, *16*, 265−269.
(78) Sun, Y.-M.; Lozano, J.; Ho, H.; Park, H. J.; Veldman, S.; White, J. M. Interfacial silicon oxide formation during synthesis of ZrO_2 on Si(100). *Appl. Surf. Sci.* **2000**, *161*, 115−122.
(79) Zhang, N. L.; Song, Z. T.; Wan, Q.; Shen, Q. W.; Lin, C. L. Interfacial and microstructural properties of zirconium oxide thin films prepared directly on silicon. *Appl. Surf. Sci.* **2002**, *202*, 126−130.
(80) Kim, M.-S.; Ko, Y.-D.; Hong, J.-H.; Jeong, M.-C.; Myoung, J.-M.; Yun, I. Characteristics and processing effects of ZrO_2 thin films grown by metal-organic molecular beam epitaxy. *Appl. Surf. Sci.* **2004**, *227*, 387−398.
(81) Li, H.; Choi, J.-I. J.; Mayr-Schmolzer, W.; Weilach, C.; Rameshan, C.; Mittendorf, F.; Redinger, J.; Schmid, M.; Rupperchter, G. Growth of an Ultrathin Zirconia Film on Pt3Zr Examined by High-Resolution X-ray Photoelectron Spectroscopy, Temperature-Programmed Desorption, Scanning Tunneling Microscopy, and Density Functional Theory. *J. Phys. Chem. C* **2015**, *119*, 2462−2470.
(82) NIST X-ray Photoelectron Spectroscopy Databse, NIST Standard Reference Database Number 20, National Institute of Standards and Technology, Gaithersburg, MD, 20899, 2000.
(83) Dupin, J.-C.; Gonbeau, D.; Vinatier, P.; Levasseur, A. Systematic XPS studies of metal oxides, hydroxides and peroxides. *Phys. Chem. Chem. Phys.* **2000**, *2*, 1319−1324.
(84) McCafferty, E.; Wightman, J. P. Determination of the Concentration of Surface Hydroxyl Groups on Metal Oxide Films by a Quantitative XPS Method. *Surf. Interface Anal.* **1998**, *26*, 549−564.
(85) Held, G.; Jones, L. B.; Seddon, E. A.; King, D. A. Effect of Oxygen Adsorption on the Chiral Pt{531} Surface. *J. Phys. Chem. B* **2005**, *109*, 6159−6163.
(86) Kim, B.-K.; Ryu, S.-K.; Kim, B.-J.; Park, S.-J. Adsorption behavior of propylamine on activated carbon fiber surfaces as induced by oxygen functional complexes. *J. Colloid Interface Sci.* **2006**, *302* (2), 695−697.
(87) Fu, X.; Wang, Y.; Wu, N.; Gui, L.; Tang, Y. Surface Modification of Small Platinum Nanoclusters with Alkylamine and Alkylthiol: An XPS Study on the Influence of Organic Ligands on the Pt 4f Binding Energies of Small Platinum Nanoclusters. *J. Colloid Interface Sci.* **2001**, *243*, 326−330.
(88) Borck, O.; Svenum, I.-H.; Walle, L. E.; Andersen, T. H.; Schulte, K.; Borg, A. Adsorption of methylamine on Ni_3Al(111) and NiAl(110)—a high resolution photoelectron spectroscopy and density functional theory study. *J. Phys.: Condens. Matter* **2010**, *22*, 395004.
(89) Wu, J.-B.; Yang, Y.-W.; Lin, Y.-F.; Chiu, H.-T. Adsorption and Decomposition Studies of *t*-Butylamine, Diethylamine, and Methylethylamine on Si(100)−(2 × 1). *J. Phys. Chem. B* **2004**, *108*, 1677−1685.
(90) Hoft, R. C.; Ford, M. J.; McDonagh, A. M.; Cortie, M. B. Adsorption of Amine Compounds on the Au(111) Surface: A Density Functional Study. *J. Phys. Chem. C* **2007**, *111* (37), 13886−13891.
(91) Brenier, R.; Mugnier, J.; Mirica, E. XPS study of amorphous zirconium oxide films prepared by sol−gel. *Appl. Surf. Sci.* **1999**, *143* (1−4), 85−91.
(92) Smirnov, M. Y.; Kalinkin, A. V.; Bukhtiyarov, V. I. X-ray photoelectron spectroscopic study of the interaction of supported metal catalysts with NO_x. *J. Struc. Chem.* **2007**, *48* (6), 1053−1060.
(93) Moulder, J. F.; Stickle, W. F.; Sobol, P. E.; Bomben, K. D. Appendix F. Atomic Sensitivity Factors for X-Ray Sources at 54.7°. *Handbook of X-ray Photoelectron Spectroscopy*; Physical Electronics Division, Perkin-Elmer Corporation, 1992; p 253.
(94) Otroschenko, T.; Sokolov, S.; Stoyanova, M.; Kondratenko, V. A.; Rodemerck, U.; Linke, D.; Kondratenko, E. V. ZrO_2-Based Alternatives to Conventional Propane Dehydrogenation Catalysts: Active Sites, Design, and Performance. *Angew. Chem., Int. Ed.* **2015**, *54* (52), 15880−15883.
(95) Otroshchenko, T.; Radnik, J.; Schneider, M.; Rodemerck, U.; Linke, D.; Kondratenko, E. V. Bulk binary ZrO2-based oxides as highly active alternative-type catalysts for non-oxidative isobutane dehydrogenation. *Chem. Commun.* **2016**, *52*, 8164−8167.
(96) Otroshchenko, T. P.; Kondratenko, V. A.; Rodemerck, U.; Linke, D.; Kondratenko, E. V. Non-oxidative dehydrogenation of propane, *n*-butane, and isobutane over bulk ZrO_2-based catalysts:

https://doi.org/10.1021/acs.jpca.2c03149
J. Phys. Chem. A 2022, 126, 7578−7590

effect of dopant on the active site and pathways of product formation. *Catal. Sci. Technol.* **2017**, *7*, 4499−4510.
(97) Jeon, N.; Choe, H.; Jeong, B.; Yun, Y. Propane dehydrogenation over vanadium-doped zirconium oxide catalysts. *Catal. Today* **2020**, *352*, 337−344.
(98) Zhang, Y.; Zhao, Y.; Otroshchenko, T.; Lund, H.; Pohl, M.-M.; Rodemerck, U.; Linke, D.; Jiao, H.; Jiang, G.; Kondratenko, E. V. Control of coordinatively unsaturated Zr sites in ZrO_2 for efficient C−H bond activation. *Nat. Commun.* **2018**, *9*, 3794.
(99) Zhang, Y.; Zhao, Y.; Otroshchenko, T.; Han, S.; Lund, H.; Rodemerck, U.; Linke, D.; Jiao, H.; Jiang, G.; Kondratenko, E. V. The effect of phase composition and crystallite size on activity and selectivity of ZrO_2 in non-oxidative propane dehydrogenation. *J. Catal.* **2019**, *371*, 313−324.

https://doi.org/10.1021/acs.jpca.2c03149
J. Phys. Chem. A 2022, 126, 7578−7590